Structural characterization of photoreduced complete and incomplete cubane-type molybdenum oxide clusters in CO and their catalytic behavior in propene metathesis reaction

Yasunori Imada [a], Takafumi Shido [a], Ryuichiro Ohnishi [a], Kiyoshi Isobe [b] and Masaru Ichikawa [a,1]

[a] *Catalysis Research Center, Hokkaido University, Kita-ku, N-11, W-10, Sapporo 060, Japan*
[b] *Department of Chemistry, Faculty of Science, Osaka City University, Izumi, Osaka 558, Japan*

Received 24 July 1995; accepted 7 December 1995

SiO_2-impregnated complete and incomplete cubane-type molybdenum oxide clusters such as $[(RhCp^*)_4Mo_4O_{16}]$ (I) and $[(RhCp^*)_2Mo_3O_9(OMe)_4]$ (II) were photoreduced with a UHP-Hg lamp (> 365 nm) in CO, resulting in the formation of catalytically active species for propene metathesis at 300 K. The CO-photoreduced Mo oxide clusters were characterized by EXAFS, IR, XPS and TPD technique. The results suggest that the Mo–O_{4c} (four-centered bridging oxygens) in I were specifically reduced with CO under the illumination to produce two sets of subcarbonyl species, e.g., those characteristic of the IR bands at 2061 and 2021 cm^{-1}, which were thermally inactive for the ^{13}CO exchange reaction but very active under illumination at 300 K, possibly assignable to $Mo(CO)_x$ ($x = 2, 3$), whereas those at 2092 and 2035 cm^{-1} due to $Rh(CO)_2$, which were readily exchangeable with ^{13}CO at 300 K in dark. Removal of both carbonyls attached on Rh and Mo in photoreduced I and II by evacuation at 375–440 K led to the formation of oxygen-deficient Mo^{4+}/Mo^{5+} sites, which exhibited high catalytic activities in propene metathesis at 300 K to produce an equimolar mixture of ethene and 2-butenes. The CO-photoreduced incomplete cubane Mo oxide cluster (II) exhibited higher activities and higher trans/cis ratios of 2-butenes in the reaction, compared with those on the photoreduced I.

Keywords: cubane-type molybdenum oxide clusters; CO-photoreduction; propene metathesis reaction

1. Introduction

Some metal/alloy cluster compounds such as $[Rh_{6-x}Ir_x(CO)_{16}]$ ($x = 0$–6) and $[Pt_3(CO)_6]_n^{2-}$ ($n = 3$–5) have been of great interest as molecular precursors grafted on oxide surfaces and entrapped in zeolite microporous cages, because of the promise of such systems for rational preparation of tailor-made metal catalysts [1,2] and quantum-dots of semiconductor devices.

Recently, novel metal oxide clusters such as integrated triple and quadruple cubane-type molybdate and vanadate cluster compounds such as $[(MCp^*)_4Mo_4O_{16}]$ and $[(MCp^*)_4V_6O_{19}]$ (M = Rh, Ir; Cp^* = pentamethylcyclopentadienyl) have been synthesized [3]. They represent a part of the stepped layer structure of (111) ordered faces of MoO_3 and V_2O_5 crystals, which are used as heterogeneous catalysts in a variety of organic oxidation reactions [4]. In particular, the structure of the complete cubane-type Mo oxide cluster I is a linear structure compound where cubic units fuse together by sharing faces, as shown in fig. 1. These oxide clusters capped with $RhCp^*$ and $IrCp^*$ gain attention as molecular modeling of the supported metal catalysts. On the other hand, the compound I reacts with MeOH in the presence of *p*-

[1] To whom correspondence should be addressed.

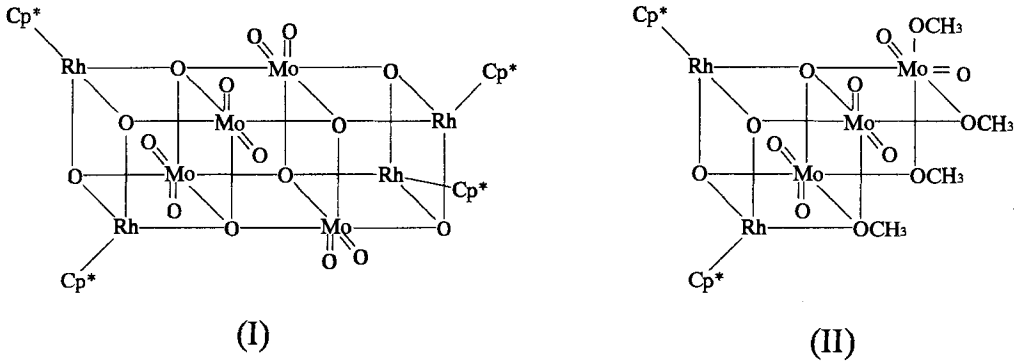

Fig. 1. Molecular structures of complete and incomplete cubane-type molybdenum oxide clusters such as $[(RhCp^*)_4Mo_4O_{16}]$ (I) and $[(RhCp^*)_2Mo_3O_9(OMe)_4]$ (II).

hydroquinone to produce incomplete cubane-type cluster II which has a cluster framework characteristic of the ordered active MoO_3 (100) faces [5]. Moreover, Kazansky et al. [6] reported that SiO_2-impregnated MoO_3 was photoreduced under CO and exhibited catalytic activity for propene metathesis, although the active structure of the Mo species was unknown. Ekerdt et al. [7] recently performed a Fourier transform IR study on the ultraviolet photoreduction of SiO_2-impregnated MoO_3 in CO to show the stoichiometric formation of carbonyl species assigned to $Mo^{4+}(CO)_2$ and $Mo^{4+}(CO)_3$.

In this study, we have used these complete and incomplete cubane-type molybdenum oxide clusters such as I and II and studied their photoreduction in CO as the molecular model of active structures for the olefin metathesis, which were characterized by means of EXAFS, XPS, TPD and FT-IR. In addition, the subcarbonyl species in the CO-photoreduced I and II have been discussed on their local structures, Mo oxidation states and catalytic activities for ^{13}CO exchange reaction and propene metathesis reaction after removal of the carbonyls by their thermal evacuation.

2. Experimental

2.1. Catalyst preparation

The cubane-type molybdenum oxide clusters I and II were synthesized and purified by the literature methods [3–5]. The Rh capped Mo oxide clusters I and II (5 wt% Rh loading) were impregnated from the CH_2Cl_2 solution at 300 K on SiO_2 gel (Aerosil 200, Japan Aerosil Co., surface area = 200 m^2/g; dehydrated by evacuation at 473 K). We represent the SiO_2-impregnated I and II as I′ and II′, respectively. The cluster-impregnated materials were photoreduced in a quartz reactor(186 ml) in CO using a ultra-high pressure (UHP) Hg-lamp (USHIO-elect. Co., USH-500D with a 500-W lamp; > 365 nm).

2.2. IR and TPD studies

Transmission infrared (IR) spectra were obtained from 200 scans at a resolution of 2 cm^{-1} with a Shimadzu-8100M Fourier transform infrared (FT-IR) spectrophotometer. The I′ powder was pressed into a self-supporting disc of 40 mg/15 mm in diameter and mounted in an IR cell with KBr windows. After evacuation at 300 K, the photoreduction was performed in CO (1.33 kPa) under illumination with an ultra high-pressure Hg lamp. Before and after the photoreduction in CO, the IR spectra were recorded at 300–573 K with subtraction of the gas phase of CO and silica background.

For the I′ after the photoreduction in CO at 300 K, the TPD (temperature-programmed desorption) study was conducted by ramping the temperature at a rate of 2 K min^{-1} from 300 to 573 K. The evolved products in TPD were monitored by an Anelva 100A quadrupole mass spectrometer.

2.3. EXAFS and XPS measurement

The samples for EXAFS measurement were mounted in in situ cells made by pyrex glass ($\phi = 15$ mm × 25 mm long) with a Kapton film (500 μm thick) to prevent exposure to air and moisture. The EXAFS spectra were measured with the BL-10B instrument of the Photon Factory in the National Laboratory for High Energy Physics (KEK-PF) using synchrotron radiation. The ring current was 360–250 mA. The EXAFS spectra were measured in transmission mode and a Si(311) channel cut monoclometer was used. Mo K-edge and Rh K-edge EXAFS spectra were analyzed using the computer program supplied by Technos Co. LTD. The EXAFS oscillation $\chi(k)$ was extracted from the observed data by subtracting the smoothly varying part, which was estimated with a Victoreen function and cubic spline method.

The k^3-weighted EXAFS function with the k-range of 3.4–15.7 Å was Fourier transformed and the Fourier transformed function was inverse Fourier transformed. The inverse Fourier transformation was conducted in the R-range of 1.08–2.27 Å, 2.55–3.23 Å, and 1.08–2.27 Å, for Mo–O, Mo–M (M = Mo or Rh), and (Rh–C and Rh–O), respectively. The Fourier filtered EXAFS function was simulated by calculated EXAFS functions which were derived from empirical backscattering amplitude and phase shift function using the single scattering plane wave theory [8,9]. The back scattering amplitude and phase shift function were extracted from those of reference compounds such as Na_2MoO_4 to evaluate the Mo–O and Rh–O contributions, whereas those for Rh–C and Mo–C were taken from $Mo(CO)_6$. Table 1 shows the crystallographic data and FT parameters of the reference compounds such as Rh, Mo foils, $Mo(CO)_6$ and Na_2MoO_4. Because the atomic numbers of Mo and Rh atoms are close to each other, we used the EXAFS parameters without any further correction. Similarly, to

Table 1
Crystallographic data characterizing the reference compounds and Fourier transform ranges used in the EXAFS analysis [a]

Sample	Crystallographic data			Fourier transform		
	shell	CN	R(Å)	Δk(Å^{-1})	Δr(Å)	n
Rh foil	Rh–Rh [b]	12	2.68	3.5–18.0	1.7–2.9	3
Mo foil	Mo–Mo [b]	12	2.75	3.5–18.0	1.8–2.6	3
$Mo(CO)_6$	Rh–C [c]	6	2.06	3.5–18.0	0.9–2.0	3
Na_2MoO_4	Mo–O [c]	4	1.77	3.5–16.0	1.1–1.7	3

[a] Notation: CN, coordination number for absorber–backscatterer pair; R, absorber–backscatterer distance; Δk, limits used for forward Fourier transformation; Δr, limits used for shell isolation (r is distance); n, power of k used for Fourier transformation.
[b] Crystal structure data from ref. [11].
[c] Crystal structure data from ref. [12].

simulate the Mo–M (M = Mo, Rh) and Rh–M (M = Mo, Rh) contributions we used the parameters from the EXAFS data of Mo foil and Rh foil, respectively. Determination of the Mo–M and Rh–Mo backscattering amplitudes for the bond length was made by comparison with those obtained in X-ray diffraction analysis [4,5]. The fitting parameters were taken from the average values for the interatomic distance (R(Å)), coordination number (CN), correction of threshold energy (ΔE_0) and difference of Debye–Waller factor ($\Delta\sigma$) from those of the reference compounds. CN was normalized using the X-ray crystallographic data of (I) and the empirical EXAFS parameter of this compound in crystal.

The error of the derived parameters was evaluated as follows: The parameter in discussion was tentatively fixed around the optimum value and the least-squares fitting was carried out by varying other parameters to calculate a residual factor. The fixed value was considered to be within the error range of the parameter if the calculated residual factor was smaller than twice that at optimum value. The error of the evaluated parameters was estimated to less than 0.04 Å for the interatomic distance and less than 30% for the coordination number, respectively.

The samples for XPS measurement were pressed into self-supporting disks (6 mm in diameter and 35 mg/cm^2 in weight) and placed and held with an Au wire (0.5 mm diameter) on the copper-rod to reduce charging of the sample. The base pressure of the UHV chamber was 1.3×10^{-9} kPa. The sample disk was illuminated in CO of 13.3 kPa by the ultra-high pressure Hg lamp through a quartz-window. The spectra of Mo_{3d} and Rh_{3d} for the fresh sample (a), reduced in CO under the photoillumination (b) and after evacuation at 473 K (c) were recorded by XPS (X-ray photoelectron spectroscopy) using the VG Escalab3-Mark II (Mg Kα $h\nu$ = 1253.6 eV, 10 kV, 10 mA). The binding energies were normalized using the reference Au wire (Au_{4f} 7/2, 5/2 = 83.8 and 87.4 eV) and the supporting SiO_2 disk (Si_{2p} = 103.8 eV) as internal standards.

3. Results and discussion

3.1. CO-photoreduction and ^{13}CO exchange reaction

Photoreduction of I′ and II′ was performed in CO at 300 K with the ultra-high pressure Hg lamp which was placed approximately 25 cm apart from the quartz cell containing the samples. About 2 mol of CO_2 per 1 mol of the Rh capped Mo_4 oxide cluster I were obtained by a prolonged photoreduction (24 h) at 300 K. As shown in fig. 2a, two sets of the carbonyl IR peaks at (2092, 2035 cm^{-1}) and (2061, 2021 cm^{-1}) were observed. All the CO peaks gradually increased and reached the maximum intensities in 24 h, as presented in fig. 2a. Interestingly, the latter twin CO stretching bands at 2061 and 2021 cm^{-1}

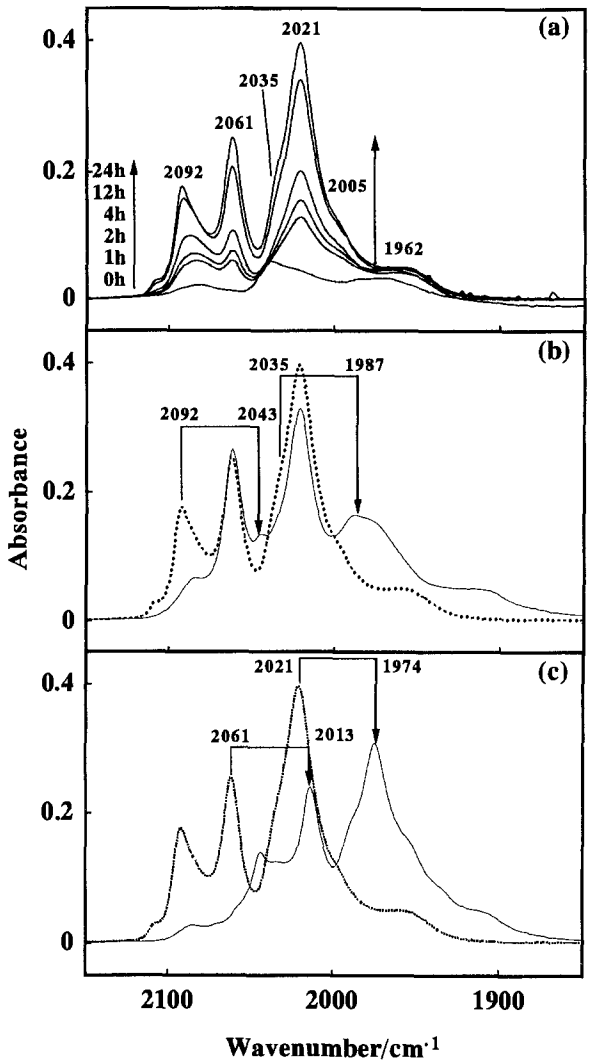

Fig. 2. IR spectral changes of I′: (a) after the photoillumination in CO at 300 K for 24 h, (b) after the CO-photoreduced sample (a) was exposed to ^{13}CO (1.33 kPa) at 300 K in 2 h and (c) after the resulting sample (b) was illuminated in ^{13}CO for 1 h at 300 K.

were substantially suppressed and eventually disappeared after thermal evacuation under 1.33×10^{-5} kPa at 373–423 K, whereas the other two bands at 2092 and 2035 cm^{-1} are thermally stable. Furthermore, it was demonstrated that the former carbonyls due to CO bands at 2092 and 2035 cm^{-1} underwent a facile exchange reaction with ^{13}CO (1.33 kPa) even at 300 K, showing the isotopic band shifts towards 2043 and 1987 cm^{-1} (fig. 2b). By contrast, the latter CO stretching bands at 2061 and 2021 cm^{-1} were thermally inactive for the ^{13}CO exchange reaction at 300–373 K, but readily reacted at 300 K under the illumination with a UHP-Hg lamp: the IR peaks were shifted to 2013 and 1974 cm^{-1}, as presented in fig. 2c. By comparison with some referred IR data of the Rh carbonyl species, e.g., $[Rh(CO)_2Cl]_2$ (ν(CO) = 2095 and 2045 cm^{-1}) and surface-grafted $Rh(CO)_2$ (ν(CO) = 2104–2085 and 2042–2035 cm^{-1}) derived from $Rh_4(CO)_{12}$ impregnated on SiO_2 and Al_2O_3 [10], the CO bands at 2092 and 2035 cm^{-1} are assigned to the twin car-

bonyls attached to Rh in the CO-photoreduced I′ as depicted in scheme 1. On the other hand, Ekerdt et al. reported [7] that the molybdenum carbonyl species are formed by ultraviolet photoreduction of MoO_3/SiO_2 in CO, showing the twin CO stretching peaks at 2128 and 2080 cm^{-1} due to the tetrahedral $Mo^{4+}(CO)_2$ species. The lower wavenumbers of CO stretching bands were also reported for the $Mo(CO)_3(OH)_3$ anchored on Al_2O_3 (2021 and 1930 cm^{-1}) [15] and $Mo(CO)_3$ in NaY pores (1911 and 1790 cm^{-1}) [16]. Accordingly, it was suggested from this evidence that the CO stretching bands at 2061 and 2021 cm^{-1} (exchangeable with ^{13}CO only under the photoillumination) are associated with carbonyls, e.g., $Mo(CO)_x$ ($x = 2, 3$) bound to the reduced Mo sites in the CO-photoreduced I′. Additionally, it was found by the FT-IR and TPD study that all the subcarbonyl species formed by the photoreduction of I′ in CO were completely removed by the evacuation at 375–440 K, possibly leaving the oxygen-deficient Mo sites as shown in scheme 1.

3.2. EXAFS/XPS characterization

In order to obtain more structural information about the photoreduction of the Rh capped Mo oxide cluster I in CO, EXAFS and XPS measurements were carried out. Fig. 3 shows the Fourier transformed k^3-weighted EXAFS function of Mo K-edge for I′ before and after the photoreduction in CO (figs. 3a–3c), and after the thermal evacuation of the CO-photoreduced sample (c) (fig. 3d). The phase shift correction was not performed in fig. 3. The major two sets of peaks were observed in figs. 3a–3d at 1.1–2.3 Å and 2.5–3.2 Å, which were attributed to Mo–O and Mo–M (M = Rh, Mo), respectively. The Mo–O contributions at 1.1–2.3 Å are reasonably resolved in three Mo–O bonds with different bond length which are reasonably assigned to the Mo=O (terminal) ($R = 1.72$ Å, CN = 2.0), $Mo–O_{3c}$ (designated as a three-centered bridging oxygen) ($R = 1.93$ Å, CN = 2.0) and $Mo–O_{4c}$ (four-centered bridging oxygen) ($R = 2.32$ Å, CN = 2.0), respectively. The contributions of $Rh–O_{4c}$ (2.10 Å) and $Rh–O_{3c}$ (2.13 Å) could not be distinguished from each other. In addition, the Mo–O–Rh ($R = 3.28$ Å, CN = 2.0) and Mo–O–Mo ($R = 3.37$ Å, CN = 3.0)) bondings were observed in the secondary coordination sphere. When the sample I′ was reduced in CO (fig. 3c), the peak at 1.8 Å before the phase shift correction relatively decreased, while the intensities of other peaks basically remained unchanged. When the CO-photoreduced sample was evacuated at higher temperatures such as 473 K, the peak intensity of Mo-metal effectively decreased and a peak at 2.4 Å, possibly due to the Mo–Mo bond, newly appeared (fig. 3d). By contrast, the peak intensity at 1.6 Å remained unchanged. Fig. 4 shows the inverse Fourier transformed EXAFS oscillation of I′ (solid line) and the calculated oscillation curve consisting of those from three Mo–O shells (dotted line) which fitted well the observed function. When the EXAFS function was simulated by one or two shells, the calculated EXAFS function cannot be adapted to the observed spectra. Table 2 summarizes the results of the curve fitting analysis of EXAFS parameters for I in crystal and I′ before and after the photoreduction and thermal evacuation of the resulting material. The Mo K-

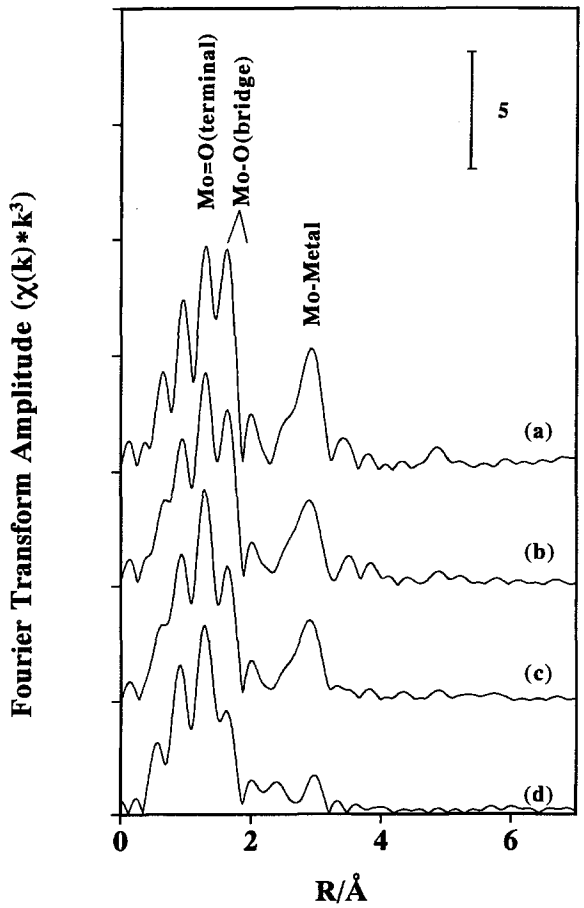

Fig. 3. Fourier transformed Mo K-edge EXAFS ($\chi(k)k^3$) for (a) I/BN, (b) I′ after evacuation at 300 K, (c) after the sample (b) was photoreduced in CO (13.3 kPa) at 300 K for 24 h, and (d) after the CO-photoreduced sample (c) was evacuated at 473 K for 2 h.

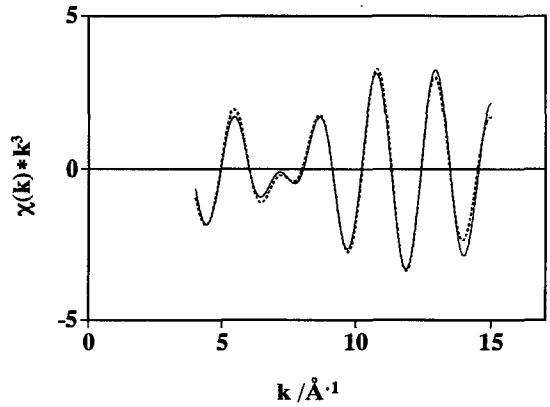

Fig. 4. Fourier filtered k^3-weighted Mo K-edge EXAFS oscillation ($\chi(k)k^3$) of I′ evacuated at 300 K (solid line), and its curve-fitting (dotted line) in the R-range of 1.08–2.27 Å for Fourier filtering.

Table 2
EXAFS results for (a) $[(RhCp^*)_4Mo_4O_{16}]$ (I) diluted in boron nitride (BN) crystal, (b) I impregnated on SiO_2 after evacuation at 300 K, (c) after photoreduction of the sample (b) in CO (13.3 kPa) at 300 K for 24 h and (d) after evacuation of the sample (c) at 473 K for 2 h to remove CO [a]

Sample	Bond	R (Å)	CN	ΔE_0 (eV)	$\Delta\sigma$ (Å)	R-factor (%)
(a) $(RhCp^*)_4Mo_4O_{16}/BN$	Mo=O(terminal)	1.73(1.70)	2.0	1.9	0.000	7.98
	Mo–O_{3c} (bridge)	1.94(1.93)	2.0	1.9	0.001	
	Mo–O_{4c} (bridge)	2.39(2.34)	2.0	1.9	0.000	
	Rh–O (bridge)	2.11(2.10)	3.0	−1.4	0.034	6.18
	Rh–C	2.15(2.13)	5.0	−5.4	0.056	
	Mo–metal (Rh)	3.28(3.22)	2.0	−4.5	0.001	7.55
	Mo–metal (Mo)	3.37(3.36)	3.0	−2.3	0.000	
	Rh–metal (Rh)	3.28(3.33)	1.0	−4.2	0.006	8.55
(b) $(RhCp^*)_4Mo_4O_{16}/SiO_2$ (evac. at 300 K)	Mo=O (terminal)	1.73	1.9	2.1	0.000	5.14
	Mo–O_{3c} (bridge)	1.94	1.7	2.1	0.020	
	Mo–O_{4c} (bridge)	2.40	1.8	2.1	0.032	
	Rh–O (bridge)	2.10	2.8	−2.8	0.037	5.97
	Rh–C	2.15	4.6	−5.0	0.050	
	Mo–metal (Rh)	3.27	1.9	−3.7	0.000	9.34
	Mo–metal (Mo)	3.38	2.6	−4.2	0.000	
	Rh–metal (Rh)	3.21	0.7	−7.2	0.005	2.19
(c) $(RhCp^*)_4Mo_4O_{16}/SiO_2$ (CO-photoreduction)	Mo=O (terminal)	1.73	1.9	1.9	0.000	6.74
	Mo–O_{3c} (bridge)	1.94	1.7	1.9	0.042	
	Mo–O_{4c} (bridge)	2.41	1.3	1.9	0.001	
	Rh–O (bridge)	2.10	2.4	−2.3	0.027	4.31
	Rh–C	2.17	5.0	−3.4	0.076	
	Mo–metal (Rh)	3.28	1.7	−3.2	0.000	8.87
	Mo–metal (Mo)	3.38	2.3	−3.6	0.000	
	Rh–metal (Rh)	–	–	–	–	
(d) $(RhCp^*)_4Mo_4O_{16}/SiO_2$ (evac. at 473 K after CO-photoreduction)	Mo=O (terminal)	1.72	1.6	0.47	0.001	6.96
	Mo–O_{3c} (bridge)	1.95	1.5	0.47	0.060	
	Mo–O_{4c} (bridge)	2.45	1.1	0.47	0.016	
	Rh–O (bridge)	2.12	1.9	−1.1	0.048	3.70
	Rh–C	2.19	5.4	−3.1	0.080	
	Mo–metal (Rh)	3.25	1.8	−2.8	0.108	10.16
	Mo–metal (Mo)	3.33	1.4	−2.0	0.037	
	Rh–metal (Rh)	–	–	–	–	

[a] CN, R (Å), E_0 (eV) and $\Delta\sigma$ (Å) represent coordination number, interatomic distance, changes in inner potential correction and Debye–Waller factor, respectively. The interatomic distances in parentheses are taken from the X-ray crystal structure data (ref. [4]). The errors in R and CN were estimated to be 0.04 Å and 30%, respectively.

edge EXAFS data suggested that the Mo–O_{4c} bond contribution was specifically suppressed ($R = 2.41$ Å, CN = 1.3) compared with those of the other Mo–O bonds after the photoreduction in CO. Additionally, it is interesting to find that according to the Rh K-edge EXAFS data for these samples, the Rh–O contribution of the Mo oxide cluster I′ was clearly decreased by the photoreduction whereas that of Rh–O (Rh–CO) remained unchanged. The subsequent thermal evacuation at 473 K to remove CO resulted in the further decrease of CN for Mo–O_{4c}, Rh–O, while the Mo–Mo bond relatively increased. Also, a slight elongation of the interatomic distances of Mo–O–metal bonds was observed, as shown in table 2. These results suggest that the bridging Mo–O_{4c} were selectively reduced by photoreduction to produce the carbonyl species which were eliminated after evacuation at 473 K. The XPS data as shown in fig. 5a suggested that the Mo in the I′ was partially reduced from Mo^{6+} (BE of Mo_{3d} 5/2, 3/2 = 234.4, 237.5 eV) to a mixture of Mo^{4+} (Mo_{3d} 5/2, 3/2 = 233.0, 236.2 eV) and Mo^{5+} (Mo_{3d} 5/2, 3/2 = 233.5, 236.7 eV) after the photoreduction in CO. Deconvolution of these peaks results in an area percentage of 41 and 11% for Mo^{4+} and Mo^{5+} (fig. 5b), respectively. Interestingly, the evacuation of the CO-photoreduced sample at 473 K led to increasing contribution (36%) of Mo^{5+}, being mixed with 18% of Mo^{4+}. The XPS results, coupled with the EXAFS/IR data suggested that the oxygen-deficient Mo^{5+}/Mo^{4+} sites are formed by removal of CO from the photoreduced oxide cluster I′, depicted as a proposed structure of I′ in scheme 1. When I′ was photoreduced in CO, an O_{4c} bridging oxygen in I′ was removed to give CO_2 ($CO + O_{4c} \rightarrow CO_2$) and carbonyls bound to the coordinatively unsaturated Mo and Rh sites. The resulting subcarbonyl species were eliminated by the evacuation at 473 K to form the oxygen-deficient Mo sites.

Kazansky [6] previously proposed a model for the

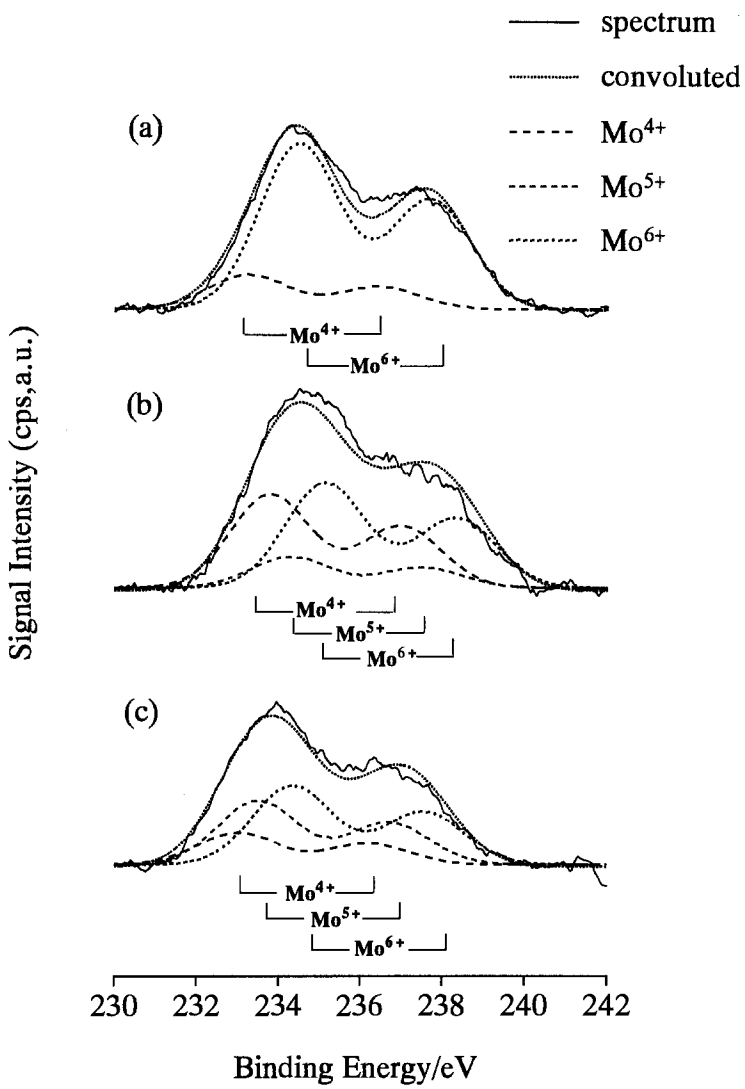

Fig. 5. Mo_{3d} XP spectra of (a) I′ after evacuation at 300 K, (b) after the sample (a) was photoreduced in CO (13.3 kPa) at 300 K for 24 h, and (c) after the sample (b) was evacuated at 473 K for 2 h.

photoreduction of MoO_3/SiO_2 catalyst in CO, which proceeds the removal of terminal Mo^{6+}=O bond to give Mo^{4+} and CO_2. By contrast, the EXAFS, FT-IR, TPD and XPS results in this work suggested that the bridged Mo^{6+}–O_{4c} bonds, whereas a negligible removal of Mo^{6+}=O bonds, are selectively reduced with CO under the photoillumination, resulting in the formation of the carbonyls attached to Rh^{3+} and Mo^{4+}/Mo^{5+} sites in the distorted cubane-type molybdenum oxide cluster frameworks. The further removal of CO eventually led to the formation of oxygen-deficient Mo^{5+}/Mo^{4+} sites with a coordinative unsaturation.

3.3. Propene metathesis reaction

Propene metathesis reaction was carried out at 273–323 K using a closed circulating system equipped with a pyrex-glass reactor with volume of 186 ml. Propene (13.3 kPa) was admitted onto the samples of I′ and II′ after the photoreduction at 300 K, followed by thermal evacuation at 473 K. Products consisting of ethene and 2-butenes were quantitatively analyzed by gas chromatography (Hitachi 163 type GC) using silica and VZ-10 columns.

Both precursor samples of I′ and II′ were inactive for the propene metathesis reaction. The reaction negligibly occurred even on the CO-photoreduced samples. Nevertheless, it was interesting to find that after the thermal evacuation at 473 K, the propene metathesis reaction occurred catalytically at 273–323 K on the CO-photoreduced I′ and II′ to yield an equimolar mixture of ethene and 2-butenes, as shown in fig. 6. The results suggested that the resulting oxygen-deficient Mo sites in the CO reduced I′ and II′ are responsible for the propene metathesis reaction, as depicted in scheme 1. Furthermore, it was found that the CO-photoreduced oxide cluster II′ exhibited over twice higher activities for the propene metathesis than the oxide cluster I′. The initial rates of

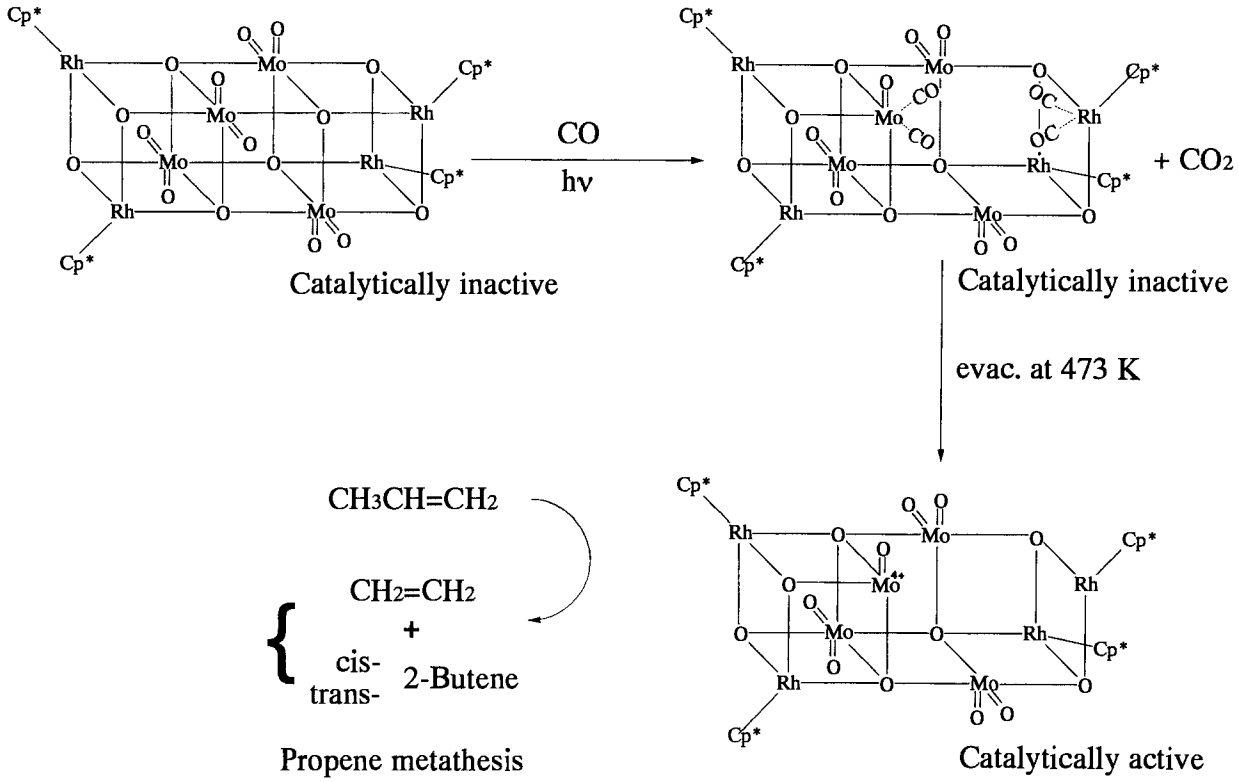

Scheme 1.

propene metathesis reaction on the CO-photoreduced I′ and II′ at 300 K were 1.75×10^{-4} and 4.15×10^{-4} mol(ethene)/(mol(cluster) s^{-1}), respectively. The CO-photoreduced I′ had much larger activation energy ($E_a = 11.2$ kJ mol^{-1}) than the II′ ($E_a = 4.8$ kJ mol^{-1}) under similar reaction conditions. The higher activities of the incomplete cubane complex II′ may be based on its higher unsaturation of coordination around Mo atoms in the oxide cluster framework, compared with those in I′ (fig. 1). Furthermore, it is noteworthy that the trans/cis molar ratios of 2-butenes formed in propene metathesis reaction on photoreduced II′ (trans/cis = 1.7) were higher than on sample I′ (trans/cis = 1.3). It may be proposed from the kinetic results that the CO-photoreduction offers more sterically crowded Mo^{5+}/Mo^{4+} sites in the complete-cubane Mo oxide cluster I for a preferable formation of trans-2-butene in the propene metathesis via the metallocyclic intermediate than the incomplete-cubane Mo oxide cluster II moieties.

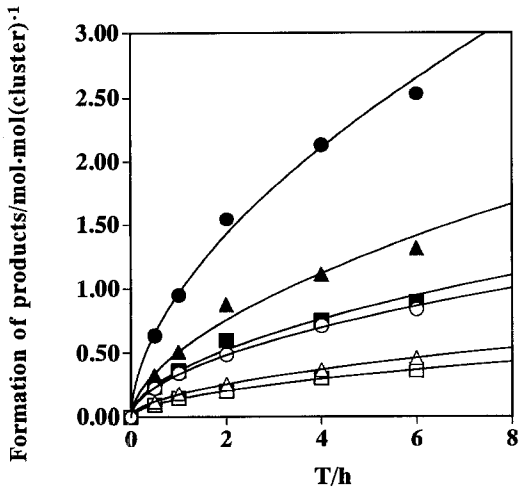

Fig. 6. Formation of products in the propene metathesis reaction at 300 K as a function of reaction time (h); (○) C_2H_4; (△) trans-2-C_4H_8, and (□) cis-2-C_4H_8 on CO-photoreduced I′, and (●) C_2H_4, (▲) trans-2-C_4H_8, and (■) cis-2-C_4H_8 on CO-photoreduced II′ after evacuation at 473 K, respectively.

Although the propene metathesis activities on the CO-photoreduced I′ and II′ were relatively smaller than those on the CO-photoreduced MoO_3/SiO_2 [6] and Mo_2(acetate)$_4/SiO_2$ [17], the activation energy of propene metathesis reaction on I′ and II′ (11.2 and 4.8 kJ mol^{-1}) were much smaller than those of the conventional Mo catalysts (20–40 kJ mol^{-1}) [6,13,14].

4. Conclusion

In summary, (1) the EXAFS, FT-IR, TPD and XPS results in this work suggested that the Mo–O_{4c} bonds in the Rh capped cubane-type Mo oxide clusters I are specifically photoreduced in CO, whereas the reduction proceeded negligibly for terminal Mo=O bonds. (2) The photoreduction of I in CO resulted in the formation of two sets of carbonyls attached to Rh^{3+} (ν(CO) = 2092 and 2035 cm^{-1}) and those with Mo^{4+}/Mo^{5+} sites (ν(CO) = 2061 and 2021 cm^{-1}). (3) All the carbonyls were completely removed by the thermal evacuation at

434 K, leaving oxygen-deficient sites which exhibited high activities for the propene metathesis reaction to form an equimolar mixture of ethene and 2-butenes. (4) The incomplete-cubane Mo oxide cluster II after the CO-photoreduction in CO provided the coordinatively unsaturated Mo sites exhibited higher catalytic activities in the propene metathesis with lower trans/cis ratio, compared with those on the complete-cubane Mo oxide cluster I.

Acknowledgement

The authors like to express thanks to Dr. H. Minagawa, Catalysis Research Center, Hokkaido University for his help to perform the XPS measurements and for valuable discussion to evaluate the BE in the XPS data analysis. The EXAFS experiments were carried out under the approval of the EXAFS program committee (Proposal No. 93G167).

References

[1] M. Ichikawa, Adv. Catal. 38 (1992) 283.
[2] M. Ichikawa, in: *Dynamic Aspects in Heterogeneous Catalysis*, ed. K. Tamaru (Plenum Press, New York, 1994) p. 149.
[3] K. Isobe and A. Yagasaki, Accounts Chem. Rev. 26 (1993) 526.
[4] Y. Hayashi, K. Toriumi and K. Isobe, J. Am. Chem. Soc. 110 (1988) 3666.
[5] Y. Do, X. You, C. Zhang, Y. Ozawa and K. Isobe, J. Am. Chem. Soc. 113(1994) 5892.
[6] V.B. Kazansky, B.N. Shelimov and K.A. Vikulov, *Proc. 10th Int. Congr. on Catalysis*, Budapest 1992, eds. L. Guczi, F. Solymosi and P. Tétényi (Elsevier, Amsterdam, 1993) p. 515.
[7] C.C. Williams and J.G. Ekerdt, J. Phys. Chem. 97 (1993) 6843.
[8] B.K. Teo, in: *EXAFS: Basic Principles and Data Analysis*, eds. C.K. Jørgensen, M.F. Lappert, S.J. Lippard, J.L. Margrave, K. Niedenzu, H. Nöth, R.W. Parry and H. Yamatera (Springer, Berlin, 1986).
[9] D.C. Koningsberger and R. Prins, in: *X-ray Adsorption*, eds. J.D. Winefordner and I.M. Kolthoff (Wiley–Interscience, New York, 1988).
[10] R. Psaro, R. Ugo, B. Besson, A.K. Smith and J.M. Basset, J. Organometal. Chem. 213 (1981) 215.
[11] R.W.G. Wyckoff, in: *Crystal Structures*, Vol. 1 (Interscience, New York, 1948).
[12] A.F. Wells, in: *Structural Inorganic Chemistry* (Clarendon Press, Oxford, 1984) p. 959.
[13] T. Takahashi, Bull. Japan Petrol. Inst. 14 (1972) 40.
[14] R. Nakamura and E. Echigoya, J. Jpn. Petroleum Inst. 10 (1976) 805.
[15] M. Laniecki and R.L. Burwell Jr., J. Colloid Interf. Sci. 75 (1980) 95.
[16] Y. Okamoto, T. Imanaka, K. Asakura and Y. Iwasawa, J. Phys. Chem. 95 (1991) 3700.
[17] M. Ichikawa, Q. Zhuang, G.J. Li, T. Fujimoto and A. Fukuoka, *Proc. 10th Int. Congr. on Catalysis*, Budapest 1992, eds. L. Guczi, F. Solymosi and P. Tétényi (Elsevier, Amsterdam, 1993) p. 529.